Volume 1 | Number 1 | Jan 2013 | Pages 1–100

Catalysis Science & Technology

www.rsc.org/catalysis

ROYAL SOCIETY OF CHEMISTRY

ROYAL SOCIETY OF CHEMISTRY

www.rsc.org/catalysis

A high effective and stable $CuZn_{0.3}Mg_xAlO_y$ catalyst for the manufacture of chiral L-phenylalaninol: The role of Mg and its hydrotalcite-like precursor

Zhangping Shi,[a] Shuangshuang Zhang,[a] Xiuzheng Xiao,[a] Dongsen Mao[a] and Guanzhong Lu[ab]*

[a] Research Institute of Applied Catalysis, School of Chemical and Environmental Engineering, Shanghai Institute of Technology, Shanghai 201418, China.

[b] Key Laboratory for Advanced Materials and Research Institute of Industrial catalysis, East China University of Science and Technology, Shanghai 200237, China.

*Corresponding Author: Fax: +86-21-64252923. E-mail: gzhlu@ecust.edu.cn (G.Z. Lu).

† Electronic supplementary information (ESI) available: The fresh, deactivated and unreduced CZA-0 catalysts were characterized by various techniques: structural and textural properties (Table S1), pore size distribution curves (Fig. S1), XRD patterns (Fig. S2), morphologies (Fig. S3), surface element compositions (Table S2), XPS spectra (Fig. S4), TG-DTG curves (Fig. S5), and the regeneration of the deactivated catalyst and its catalytic activity. See DOI: 10.1039/b000000x/

Abstract: A high-effective $CuZn_{0.3}Mg_xAlO_y$ (x = 0~0.2) catalyst for the synthesis of chiral L-phenylalaninol derived from Cu-rich hydrotalcite-like precursors were prepared by a co-precipitation method with Na_2CO_3 precipitant, and their physicochemical and catalytic properties were characterized. The results show that the presence of Mg^{2+} ions can promote the formation of hydrotalcite-like (htl) precursors, and the Mg^{2+} content would affect the phase purity of prepared htl precursor. The BET surface area, exposed copper surface area and the amount of acid sites of sample were decreased with the increase in the molar ratio of Mg^{2+}/Al^{3+}. And the dense layered htl precursors are beneficial to the atomically uniform distribution of corresponding metal oxides in the prepared catalysts, promoting the stronger interaction between Cu^0 and Al_2O_3 after the catalyst was reduced (SMSI effect). The activity of the $CuZn_{0.3}Mg_xAlO_y$ catalyst is not only greatly dependent on the metallic copper surface area, but also the SMSI effect and the acidity of the catalysts. When Mg^{2+}/Al^{3+} = 0.1(mol), the phase-pure htl precursor could be obtained, and after calcination the prepared CZA-0.1 catalyst exhibited very excellent catalytic performance for the hydrogenation of

L-phenylalanine methyl ester to chiral L-phenylalaninol. After 5h of the reaction at 110 °C and 4 MPa of H_2, 100% conversion of L-phenylalanine methyl ester and 91.1 % yield of L-phenylalaninol with *ee* value of ~100% were achieved. After recycling utilization 13 times, the L-phenylalaninol selectivity of the CZA-0.1 catalyst was only decreased by 7.2%.

1. Introduction

Chiral amino alcohols, especially L-phenylalaninol, are an important kind of small chiral molecules, and widely used in pharmaceutical and materials chemistry, resolution of racemic mixtures and asymmetric organic synthesis, *etc.*[1-8] Hence, the manufacture of chiral amino alcohols is the subject of considerable interest. Like most of chiral amino alcohols, L-phenylalaninol can be prepared by reducing the corresponding acids or esters with metal hydrides as the reducing agents, which are reactive at low temperature thereby guaranteeing the integrity of the stereogenic center [9-12]. However, most of these metal hydrides are only used in the laboratory to produce chiral amino alcohols on a 100-150 g scale, and the high costs and large amount of waste make this methodology less attractive for the commercial application. Undoubtedly, seeking a new synthetic route with absence of these drawbacks seems increasingly attractive and imperative. Recently, we have developed a new and environmentally friendly approach to synthesize L-phenylalaninol by the catalytic hydrogenation of L-phenylalanine methyl ester over the $Cu/ZnO/Al_2O_3$ catalyst, and 83.1 % yield of L-phenylalaninol without racemization was achieved under relatively mild reaction conditions [13,14], which has – to the best of our knowledge – never been reported. However, the L-phenylalaninol selectivity and stability still can be further improved for an industrial application, and the structure-activity relationship of catalyst for this title reaction is also ambiguous.

Nowadays, the $Cu/ZnO/Al_2O_3$ catalysts have been popularly studied and used in many hydrogenation reactions.[15-17] Many reports are related to the empirical optimizations for the catalyst preparation based on the given reaction, such as the aging time, preparation methods and parameters, calcination and reduction condition, *etc*. However, a general and comprehensive regulation is hardly

established on the preparation of $Cu/ZnO/Al_2O_3$ catalyst, because various factors are complex to influence the structural characteristics and physicochemical properties of obtained catalysts, and finally affect their catalytic performance. Recently, the investigations on the structure of precipitated intermediates, namely the precursors of the composite metallic oxides, have revealed that some specific precursor phases play important roles on the catalytic performance of Cu-based catalysts. For the $Cu/ZnO/Al_2O_3$ catalyst, various individual precursor phases were reported, such as, zincian malachite,[18,19] aurichalcite,[20] rosasite,[21] hydrotalcite-like (htl),[22-24] *etc*. This contribution focused on the preparation of $Cu/ZnO/Al_2O_3$ by the help of the hydrotalcite-like precursor.

It is well known that the CuZnAl htl compound is a typical kind of layered double hydroxides (LDHs) with the general formula $[M^{2+}_{1-x}M^{3+}_x(OH)_2]^{x-}(A^{n-})_{x/n}\cdot mH_2O$, where M^{2+} and M^{3+} are the divalent and trivalent cations and A^{n-} represents the anion.[24,25] In the layered structure, all the three metal species share the octahedrally coordinated sites. After calcination, the formed homogeneous micro- and nano-structure crystallites can disperse highly in the composite oxide catalysts, and promote the interaction between the corresponding metal oxides. Unfortunately, the $CuM^{2+}M^{3+}$ htl precursor materials can be only obtained when the ratio of Cu/M^{2+} is ≤ 1.[26-28] This can be attributed the higher Jahn-Teller distortions of the MO_6 octahedra in the htl crystal structure as the Zn^{2+} ions (d^{10}, no Jahn-Teller distortion) gradually substituted by Cu^{2+} ions (d^9 Jahn-Teller distorted coordination), which can destabilize the htl structure. To the best of our knowledge, in the $Cu/ZnO/Al_2O_3$ catalyst prepared by co-precipitation method with sodium carbonate as a precipitant, the optimal and typical ratio of Cu/Zn was 2−3 with 10−20 % Al.[19,29] Hence, the synthesis of phase-pure Cu-rich htl materials should be a difficult challenge.

Mg/Al hydrotalcite is the typical LDHs compounds and synthesized easily in a wide range of compositions by the co-precipitation method with Na_2CO_3 precipitant.[30] And the Mg^{2+} ions can be substituted by Cu^{2+} and Zn^{2+} ions in the htl compounds, because they have the similar ionic radius. Herein, we tried to use the Mg^{2+} ions as "ion inducer" to introduce Cu^{2+} and Zn^{2+} into the layered structure and prepare phase-pure Cu-rich $CuZn_{0.3}Mg_xAl$ htl precursors, and after calcination the high effective $CuZn_{0.3}Mg_xAlO_y$ (x = 0 ~ 0.2) catalysts for the hydrogenation of L-phenylalanine methyl

ester to L-phenylalaninol (Eq. 1) was prepared. The effect of adding Mg amount on the structure characteristics and physicochemical properties of this $CuZn_{0.3}AlO_y$ was studied, which affected its catalytic performance and usage stability. Based on these research results, the role of Mg and hydrotalcite-like precursor on improving the catalytic performance was discussed in detail.

$$\text{(1)}$$
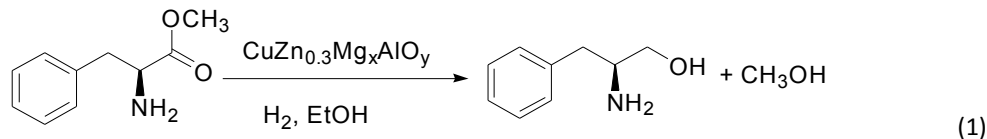
2. Experimental section

2.1. Catalyst preparation

The $CuZn_{0.3}Mg_xAlO_y$ (x = 0, 0.05, 0.1, and 0.2) catalysts were prepared by the co-precipitated method with $Cu(NO_3)_2 \cdot 3H_2O$, $Zn(NO_3)_2 \cdot 6H_2O$, $Al(NO_3)_3 \cdot 9H_2O$, $Mg(NO_3)_2 \cdot 6H_2O$ and Na_2CO_3 (A.R., Sinopharm Chemical Reagent Co. Ltd.), and the preparation procedures are described as follows. 1.0M $Cu(NO_3)_2$, 1.0M $Zn(NO_3)_2$, 1.0M $Al(NO_3)_3$, 1.0M $Mg(NO_3)_2$ and 0.5M Na_2CO_3 aqueous solutions were prepared, respectively. The mixed aqueous solution of Cu^{2+} and Zn^{2+} nitrates and 0.5M Na_2CO_3 solution were co-precipitated at 70 °C under stirring. During the precipitation process, the flow rates of two solutions were adjusted to given a constant pH value of 7.5. And the mixed aqueous solution of Mg^{2+} and Al^{3+} nitrates and 0.5M Na_2CO_3 solution were co-precipitated under the same conditions described above. Then, two mixed solutions obtained above were mixed under the same condition, this synthesis solution were aged under stirring for 2 h, and cooled statically for 1h. After filtration and washing with de-ionized water until the filtrate was neutral, the synthesized precursor material was dried at room temperature for 12 h, then dried at 120 °C for 24 h, and heated to 450 °C at 5 °C/min and calcined at 450 °C for 4 h. The calcined sample was pressed and crushed to small-sized particles of 0.45–0.85 mm (20–40 mesh). The catalyst was marked as CZA-Mg$_x$ (Mg$_x$ = 0, 0.05, 0.1, and 0.2), and the corresponding MgO content was 0, 2.1, 4.2 and 7.7 mol.%.

2.2. Catalyst characterization

The powder X-ray diffraction (XRD) patterns of catalysts were recorded on a PANalytical X'Pert Pro MRD X-ray diffractometer (Netherlands) with CuKα radiation (λ = 0.154056 nm) operated at 40

kV and 40 mA. The surface areas (S_{BET}) of catalysts were measured by N_2 adsorption at −196 °C on a Micrometrics ASAP 2020 apparatus and calculated by the Brumauer–Emmett–Teller (BET) method. Before testing, the sample was degassed at 200 °C for 10 h. Transmission electron microscopy (TEM) images of samples were obtained on a JEOL 2100 microscope operated at 100 kV. The samples were suspended in ethanol and supported onto a holey carbon film on the Cu grid. Scanning electron microscopy (SEM) images of samples were taken on a Nova NanoSEM 450 scanning electron microscope operated at 5 kV. Thermo-gravimetric/differential scanning calorimetry (TG/DSC) analyses of samples were performed on a TGA Q5000 IR Thermogravimetric analyzer at a heating rate of 10 °C/min from 30 to 800 °C in N_2 or air flow (30 mL/min).

H_2-temperature-programmed reduction (H_2-TPR) was performed on a continuous-flow apparatus equipped with a thermal conductivity detector (TCD). 30 mg catalyst was used and pretreated at 350 °C for 1 h under N_2 flow of 30 mL/min. After being cooled to 50 °C under N_2, the catalyst was flushed with 10% H_2/N_2 of 30 mL/min instead of pure N_2, and TPR of sample was run from 50 to 550 °C at 5 °C/min.

Temperature-programmed desorption of NH_3 adsorbed on the catalyst (NH_3-TPD) was carried out in a conventional flow system equipped with a thermal conductivity detector (TCD). 100 mg sample was used and pretreated in N_2 at 450 °C for 1 h. After it was cooled to 100 °C under a N_2 flow, the sample adsorbed NH_3 at 100°C for 1 h under 10 %NH_3/N_2 (30 mL/min), and N_2 purged the sample for 2 h to remove the physically adsorbed NH_3. After that, the NH_3-TPD experiments were carried out at 100–800 °C in a flow of N_2 (30 mL/min). The rate of heating was 5 °C/min.

The metallic copper surface area (S_{Cu}) of the catalyst was determined by using a nitrous oxide chemisorption method called reactive frontal chromatography (RFC) technique [31]. For example, 200 mg sample was reduced in 5 % H_2/He stream at a heating rate of 5 °C/min to 300 °C and maintained for 1 h. After that, the reactor was purged with the pure He stream and cooled down to 60 °C, and then the N_2O titration was carried out. The surface copper atoms density of 1.46×10^{19} copper atoms per m^2, $Cu/N_2O = 2/1$ was used for the calculation of the copper surface area. Additionally, the dispersion of metallic copper (D_{Cu}) was defined as the amount of the exposed copper in relation to

the total amount of copper atoms of the catalyst.

2.3. Raw material preparation

Raw material, L-Phenylalanine methyl ester, was obtained from L-phenylalaninate by the reaction formula Eq.(2). L-Phenylalaninate was dissolved in de-ionized water, and then adjusted pH to ~8 by adding sodium carbonate solution. After extraction with ethyl acetate, the extract was dried by anhydrous magnesium sulfate for 30 min. After filtration, L-Phenylalanine methyl ester was obtained by rotary evaporation.

$$ (2) $$
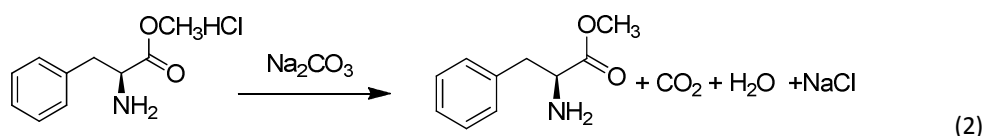
2.4. Catalytic activity testing

The catalytic activity of the catalyst for L-phenylalanine methyl ester (L-p) hydrogenation was tested in a 500 mL stainless steel autoclave under stirring at a speed of 500 rpm. After 1.0 g catalyst (20-40 mesh) was putted into the reactor, this reactor was flushed with 4 MPa H_2 to expel air 4 times and the catalyst was reduced in 1 MPa H_2 at 250 °C for 4 h, and then the reactor was cooled to room temperature. 1.5 g L-p diluted in 150 mL ethanol was introduced, that is, L-p/Cat.=1.5 (mass ratio). The typical reaction conditions were 4MPa of H_2 and 110 °C. After the reaction was over, the reactor was cooled to room temperature, and then the pressure was released. The catalyst was separated by centrifuging, and the products were analyzed by the HPLC, and ^{1}HNMR (Bruker, AVANCE III 500 MHz).

HPLC (High Performance Liquid Chromatography) analysis was measured on an Agilent 1260 Infinity equipped with an ultraviolet detector and a column (Poroshell 120 EC-C18, 50 × 4.6 mm, 2.7 μm particle size). The operated conditions of HPLC were as follows: mobile phase was 0.05 mol/L ammonium acetate aqueous solution (pH = 5.0) containing 5 vol.% methanol and the flow rate was 0.6 mL/min, detection wavelength was 254 nm and the column temperature was 35 °C. Experimental errors for the conversion and selectivity were within ±2%. The conversion of L-phenylalanine

methyl ester (X)，yield (Y) and chemselectivity (S) of L-phenylalaninol (L-p-ol) were calculated as follows:

X(%) = (the mass of L-Phenylalanine methyl ester converted/total mass of L-Phenylalanine methyl ester in the feed) × 100 %

Y(%) = (themass of L-phenylalaninol formed actually/the mass of L-phenylalaninol formed theoretically) × 100 %

S (%) = (Y/X) × 100 %

The ee value of the product was determined by the HPLC with a chiral column (CHIRALPAK ID-3, 150 × 4.6 mm, 5μm particle size) under the operation conditions: mobile phase was the mixture solution (water/methanol = 70: 30 (v/v), 0.6 mL/min) containing 3% triethylamine, detection wavelength was 258 nm and the column temperature was 40 °C.

2.5. The structure and ee value of product

The ^{1}H NMR spectrum of product L-phenylalaninol was obtained on a Bruker AVANCE-III 500. ^{1}HNMR(CDCl$_3$): 7.21~7.35 (5H, m, Ph-H), 3.42~3.68 (2H, m, -CH$_2$-O-), 3.15 (1H, s, -CH-N-), 2.53~2.84 (2H, m, CH$_2$-Ph), 1.83 (2H, b, -NH$_2$). In the product solution, only L-phenylalaninol could be detected by the HPLC with a chiral column, which indicates that the ee value is ~100% and a chirality of the reactant can be well maintained after the reaction.

3. Results and discussion

3.1. Textural and structural properties of catalysts

The XRD patterns of as-synthesized catalysts are shown in Fig.1. When Mg^{2+}/Al^{3+} molar ratio was 0.1, pure-phase hydrotalcite-like (htl) was successfully synthesized, which are corresponding to the typical XRD pattern of hydrotalcite-like. The samples with the Mg^{2+}/Al^{3+} ratio of 0.05 and 0.2 exhibited the htl structure along with another phase with four diffraction peaks at 2θ = 14.5, 17.5, 31.8 and 32.7º, which is ascribed to zincian malachite. [26,32] For the CZA-0 sample without Mg^{2+} ions, the malachite phase with low crystallinity could be observed. Additionally, it can be seen that the

diffraction peaks of htl phase became stronger and sharper with increasing Mg^{2+} amount, indicating an increase in the crystallinity of the htl phase.
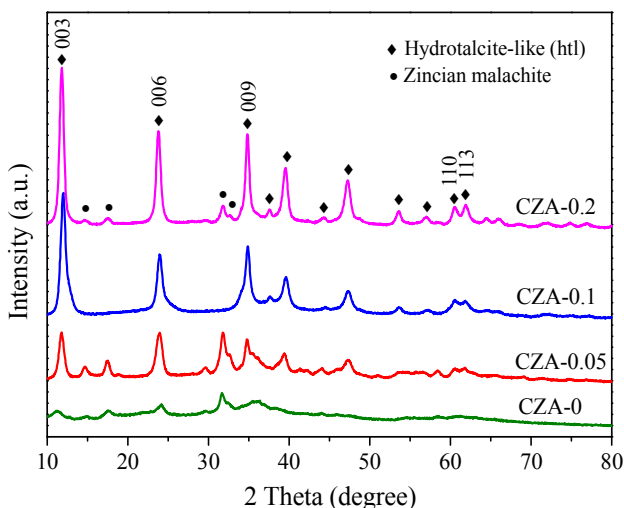

Fig. 1. XRD patterns of as-synthesized CZA-Mg_x catalysts with different Mg^{2+} amounts.

To investigate the decomposition of the precursor materials during the calcination, TG and DSC techniques were used, and the results are shown in Fig. 2. In the TG curve of the CZA-0.1 sample with hydrotalcite-like phases, there are three major weight losses: the first weight loss at 100−200 °C can be attributed to an elimination of physically adsorbed and interlayer water, the second weight loss at 200−350 °C is smaller and can be ascribed to the dehydroxylation in the hydrotalcite-like layers as well as the removal of CO_2 from the decomposition of interlayer carbonate,[25,33] resulting in the collapsing of the htl crystal structure, and the third weight loss at 600−700 °C can be assigned to decomposition of Cu oxocarbonates formed.[25,34] In the DSC curve of CZA-0.1 sample, there is a sharply endothermic peak at ~150 °C, which involved the elimination of the interlayer crystal water.[35,36] The curves of CZA-0 sample are different from the other three samples, which is presented as the malachite phase with low crystallinity. In its TG curve, the first weight loss at 100–400 °C should be attributed to the loss of physically adsorbed water and the decomposition of amorphous Cu-containing hydroxyl carbonates. And the second weight loss at 450–550 °C should be ascribed to the decomposition of Cu/Zn hydroxocarbonates, which is similar to the third weight loss of CZA-0.1. For the CZA-0.05 sample, it contained the mixed phases of hydrotalcite-like (htl) and zincian malachite, and its DTG and DSC curves were composed of the curves of CZA-0 and

CZA-0.1, but its top-temperatures have been changed. And for the CZA-0.2 sample, its dominant phase is CZA-phase with minor zincian malachite crystallites, so that its curves of TG, DSC and DTG are similar to these of the CZA-0.1 sample, which are ascribed to the decomposition of Cu/Zn hydroxocarbonates.
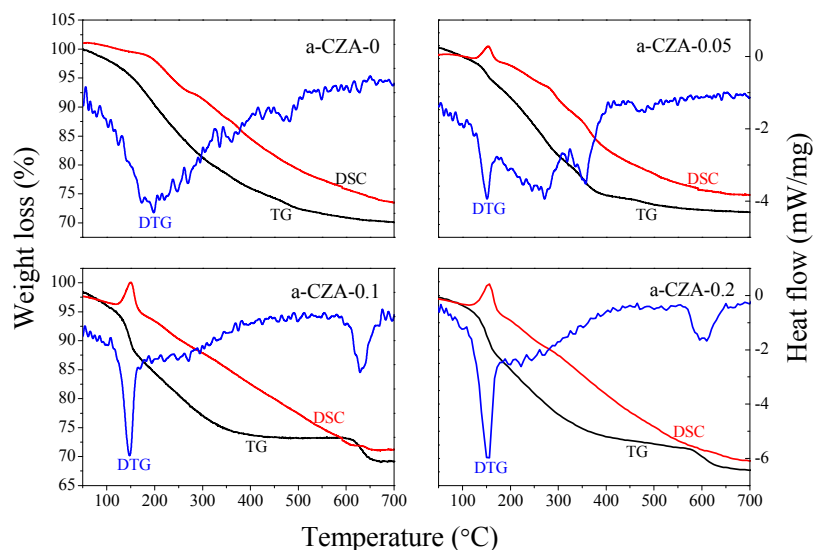

Fig. 2. TG-DTG-DSC curves of as-synthesized CZA-Mg$_x$ samples with different Mg^{2+} amounts.
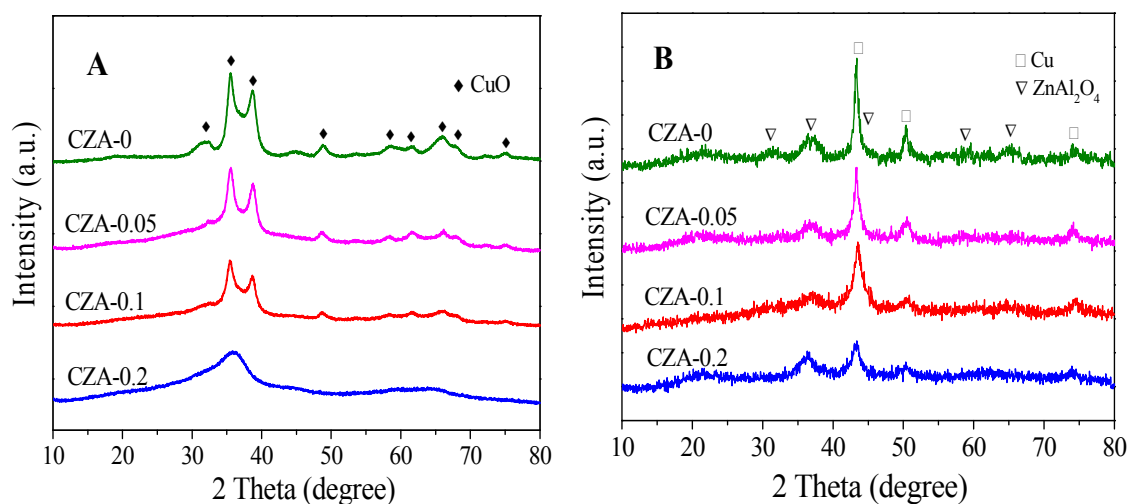
Fig. 3. XRD patterns of the CZA-Mg$_x$ catalysts (A) calcined at 450 °C and (B) after in-situ reduction.

As shown in the XRD patterns of Fig. 3A, after the as-prepared samples were calcined at 450 °C, the similar crystal structures were obtained for the all samples, in which CuO was the dominant phase and no diffraction peaks of ZnO, MgO and Al$_2$O$_3$ could be detected, that is to say, those oxides in the calcined catalyst are highly dispersed. Evidently, the diffraction peaks of hydrotalcite-like (htl) phases have disappeared in the calcined catalysts, which mean that the heat treatment would destroy

the htl structure. And with the increase in the Mg^{2+}/Al^{3+} molar ratio, the CuO reflection peaks of the all samples became weaker and boarder, which indicates a decrease of CuO crystal size and crystalline degree. Correlating the intensities of the CuO diffraction peaks with the thickness of layered htl platelets obtained by the SEM images (Fig. 4), it can be found that, the larger the thickness of htl layered precursor materials, the lower crystalline degree of copper oxide produced is. After these four catalysts were *in situ* reduced at 1 MPa H_2 at 250 °C for 4 h, the characteristic diffraction peaks of spinel structure $ZnAl_2O_4$ phase (ICDD 5-669) and Cu^0 phase could be observed in their XRD patterns (Fig. 3B), while the CuO reflection peaks disappeared, which shows that CuO is completely reduced to metallic copper and $ZnAl_2O_4$ phase can be formed after reduction. Obviously, the Cu^0 reflection peaks become weaker and boarder with the increase in the Mg^{2+}/Al^{3+} molar ratio, that is, a decrease of Cu^0 crystal size and crystalline degree. These results suggests that the doping of Mg^{2+} can decrease the crystal size and increase the dispersion of the Cu^0 species with the aid of the formation of the hydrotalcite-like (htl) precursor.

The SEM images of as-prepared and calcined CZA-Mg_x catalysts are given in Fig. 4. It can be seen that the structure of CZA-0 precursor is irregular particles. After doping Mg^{2+} ions, the morphology of CZA precursor was varied. The CZA-0.05 precursor exhibited two different types of microstructure: its major part comprised needle-like crystallites, and minor amounts are platelet-like crystallites. According to the research results of Behrens *at al*., the needle-like crystallites can be ascribed to the zincian malachite phases in the precursor materials.[18,19] And the appearance of platelet-like crystals shows the formation of layered htl phases.[24-26] With the increase in the molar ratio of Mg^{2+}/Al^{3+}, the needle-like crystallites disappeared, and only well-developed and thin platelet-like crystallites were presented in the CZA-0.1 precursor with a size of 100−200 nm, which were homogeneous and dense stacking. When more Mg^{2+} ions were introduced into the sample (as CZA-0.2), some fragments formed, and its size and thickness of platelets increased markedly. It was reported that the smaller crystal size of the htl platelets favors face-to-face and edge-to-edge interaction between individual platelets, because of the higher surface energies.[37]

After the CZA-Mg$_x$ precursors were calcined at 450 °C, the CZA-0.1 and CZA-0.2 samples roughly maintained the morphologies of the precursor materials, though some crystallites have been destroyed during a thermal treatment, indicating that the layered structure have a good thermal stability, and the particles aggregation would not occur after the thermal treatment.
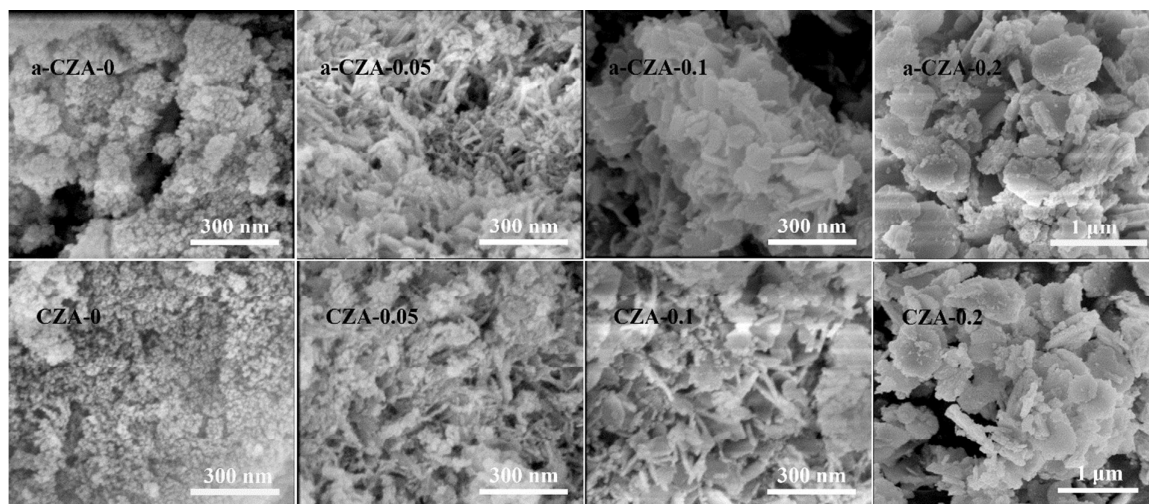

Fig. 4. SEM images of as-prepared (a-) and calcined CZA-Mg$_x$ catalysts.

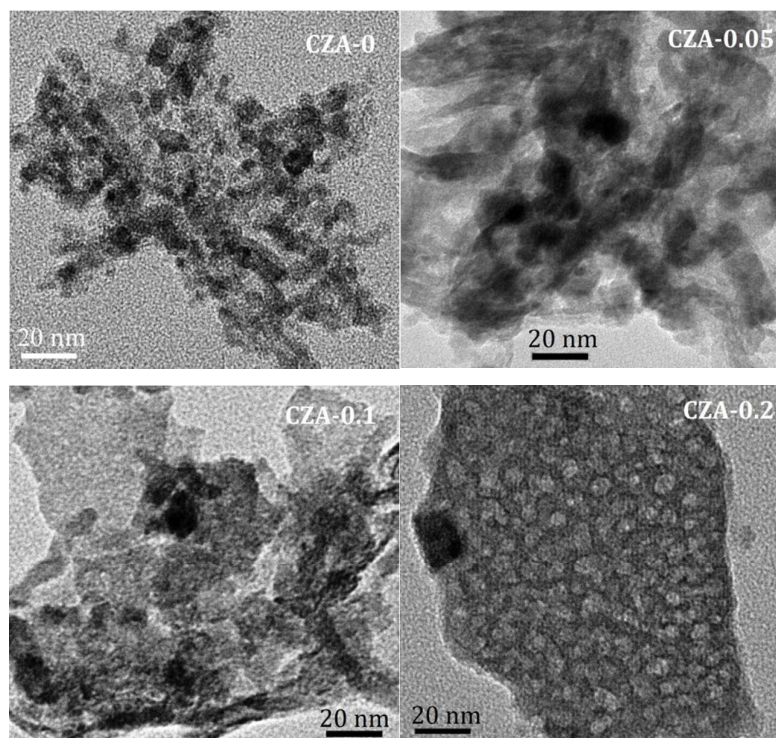Fig. 5. TEM images of the CZA-Mg$_x$ calcined at 450 °C.

The TEM images of the catalysts with different ratios of Mg^{2+}/Al^{3+} are shown in Fig. 5. CZA-0 and CZA-0.05 samples exhibited the similar morphology (approximately granular pattern) with the

crystallite size of 10−20 nm. For the CZA-0.1 sample, unlike former two samples, some lamellar platelets with size of 50−80 nm can be observed, and a small amount of isolated and agglomerated particles located on the destroyed platelets. Similarly, for the CZA-0.2 sample, only thick platelet-like particles can be observed, and the thickness and size are much larger than that of CZA-0.1 sample, which are consistent with the SEM images presented in Fig. 4.

3.2. The reducibility of catalysts

To assess the reduction behavior of the calcined catalysts, H_2-TPR technique was used and the results are shown in Fig. 6. The reduction peaks of all samples are located at 150−300 °C, which can be deconvoluted into two (α and β) peaks. The peak positions and the relative contribution of α peak to the TPR pattern are summarized in Table 1. Since ZnO, MgO and Al_2O_3 cannot be reduced in this temperature region,[26,31,38,39] these reduction peaks are only ascribed to the reduction of CuO species.

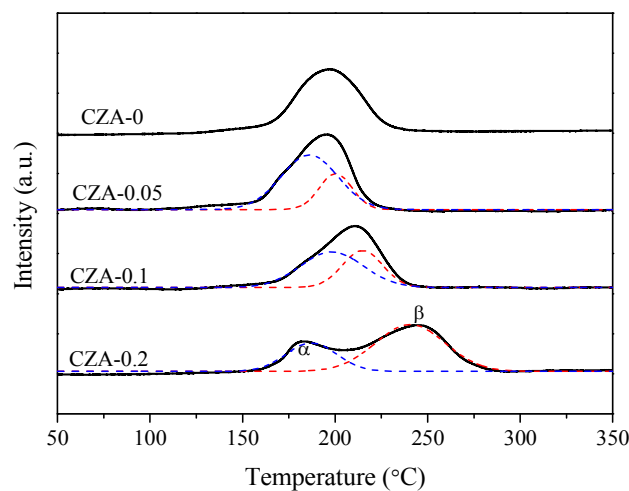**Fig. 6.** H_2-TPR profiles of the CZA-Mg_x calcined at 450 °C.

Table 1. The top temperatures of reduction peaks and their contributions in TPR patterns of calcined catalysts.

Sample	$T_α$ (°C)	$T_β$ (°C)	$A_α/(A_α+A_β)$ [a] (%)
CZA-0	196	–	100
CZA-0.05	186	200	72.5
CZA-0.1	197	215	60.1
CZA-0.2	187	240	30.6

[a]A is reduction peak area.

In the TPR curve of the CZA-0 sample, only one reduction peak existed at ~196 °C, suggesting that uniform particles of CuO species are presented. After doping Mg^{2+} ions, the reduction peak of the calcined catalysts split into α and β peak. The low temperature reduction peak (α peak) of the three samples have the similar top temperature, and should be the reduction peak of nanosized CuO clusters exposed in the surface of platelets [26] or surface CuO. Tan *et al.*[44] reported that the strong interaction between the CuO and Al_2O_3 could make the H_2 reduction temperature of copper oxide be much higher than that of supported CuO. Li *et al.*[45] reported that the intergrowth mixed oxides of CuO and γ-Al_2O_3 have strong mutual interaction, which can make the H_2 reduction temperature be higher than the mechanically mixed oxide.

Herein, the doping of Mg^{2+} ions can promote the formation of hydrotalcite-like (htl) phase in precursor materials, which is beneficial to the distribution of corresponding metal oxides in an atomic level. The high dispersed nano-Cu^{2+} species could incorporate into the Zn-Al-O matrix after being calcined,[46] resulting in a segregation of reducible Cu^{2+} before reduction from irreducible Zn^{2+} and Al^{3+} species. Hence, the higher temperature reduction peak (β peak) should be attributed to the well-dispersed Cu^{2+} cations,[46] and was increased with the increase in the crystallinity of htl phases accompanied by a decrease in the fraction of α peak (Table 1). Although this strong incorporating effect results in the reducibility decline of the Cu^{2+} species, it can help to increase and stabilize the Cu^0 dispersion by the introduced the strong metal-support interaction (SMSI) effect between Cu^0 with Al_2O_3 after catalyst reduction, increasing the catalytic performance and stability of this catalyst. For the CZA-0 sample without Mg doping, the growth of the metallic copper crystallite during the reaction (TEM images, Fig. S3) is responsible for the deactivation behavior of the CZA-0 sample.

The BET surface areas (S_{BET}) of the calcined catalysts are listed in Table 2. Some decrease of S_{BET} can be observed after adding Mg in CZA, and when $Mg^{2+}/Al^{3+} = 0.2$ (CZA-0.2), its surface area was obviously decreased to from 92 m^2/g to 58.1 m^2/g. The layered structure makes the metallic oxides intimate contact each other, which will reduce the volume of the piled pores. And the thicker the layered structure thickness, the more obvious this effect should be.

Table 2. Physicochemical properties of the CZA-Mg$_x$ calcined at 450 °C.

Sample	S_{BET}(m^2/g)	S_{Cu}(m^2/g)[a]	S_{Cu}/S_{BET}(%)	D_{Cu}(%)[b]
CZA-0	92.0	16.9	18.4	8.1
CZA-0.05	86.6	14.0	16.2	6.8
CZA-0.1	88.8	7.5	8.5	3.7
CZA-0.2	58.1	3.2	5.5	1.6

[a] S_{Cu} was determined by N_2O adsorption. [b]D_{Cu} = exposed Cu atoms/total Cu atoms.

The accessible metallic copper surface area (S_{Cu}) of the calcined catalysts was determined by N_2O titration after reduction. The effect of Mg^{2+}/Al^{3+} ratio on S_{Cu} is similar to S_{BET}. As shown in Table 2, S_{Cu} of CZA-0.2 is only 3.2 m^2/g, and is 5.5% of its BET surface area of 58.1 m^2/g. With the decrease of the Mg amount in CZA-Mg$_x$, its S_{Cu} (or S_{Cu}/S_{BET}) was enhanced, such as, S_{Cu} of CZA-0 was maximum (16.9 m^2/g), and reached 18.4% of its S_{BET}. For the CZA-0.1 catalyst, its S_{Cu} was 7.5 m^2/g and 18.4% of its S_{BET} (88.8 m^2/g). This is because that dense layered structure of the calcined catalyst resulted from the htl precursor materials would make the Cu particles embed in a compact oxide matrix to a large extent; hence, the accessible Cu surface areas of these calcined samples are much lower than that of the $CuZn_{0.3}AlO_x$ catalyst.

3.3. The surface acidities of $CuZn_{0.3}Mg_xAlO_y$ catalysts
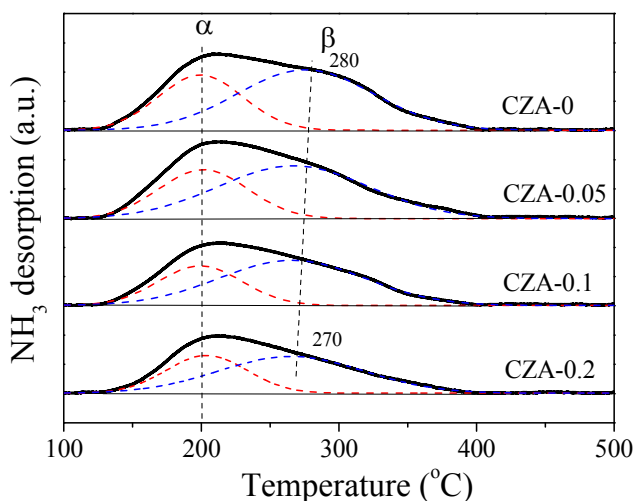
Fig. 7. NH$_3$-TPD profiles of the CZA-Mg$_x$ calcined at 450 °C.

The acidities of the $CuZn_{0.3}Mg_xAlO_y$ catalysts were determined by NH_3-TPD, and the results are shown in Fig. 7. As shown in Fig.7, four TPD profiles have the similar broad peak that can be deconvoluted into two (α and β) peaks, and the former was located at ~200 °C and the latter was located at 270−280 °C, which can be ascribed to the weaker and middle-strong acidic sites, respectively. These acid sites are related to the contribution of different metal oxides, such as Al_2O_3, ZnO, CuO, in which the contribution of Al_2O_3 is probably prevailing. With an increase in the MgO amount, the intensities of α and β peaks were gradually decreased, which means the reduction of the weaker and middle-strong acid site amounts. Thus, MgO can act as an effective dopant to adjust the acidic sites over the $Cu/ZnO/Al_2O_3$ catalyst.[47,48] To quantify these changes, the TPD profiles were integrated, and the results are listed in Table 3. The following characteristics can be obtained: (1) the amounts of meddle-strong and weaker acid sites are continuously decreased with Mg^{2+}/Al^{3+} ratio increasing from 0 to 0.2; (2) the strength of the weaker acid sites is hardly affected by the ratio of Mg^{2+}/Al^{3+} because of the unchanged α peak temperature; (3) the strength of the meddle-strong acid sites is dropped a little with increasing Mg^{2+} amount; (4) the fraction of weaker or meddle-strong acid sites to total acidity sites is hardly affected by the ratio of Mg^{2+}/Al^{3+}; (5) the density of total acid sites of CZA-0.1 sample is the smallest.

Table 3. The positions and areas of the NH_3 desorption peaks.

Sample	T_α/T_β (°C)	Total acid sites			
		(μmol/g)	(μmol/m²)	α (μmol/g)	β (μmol/g)
CZA-0	200/280	13.3	0.145	4.7 (35.2%)*	8.6 (64.8%)
CZA-0.05	200/276	12.0	0.138	4.4 (34.6%)	8.2 (65.4%)
CZA-0.1	200/273	10.3	0.116	3.5 (34.0%)	6.8 (66.0%)
CZA-0.2	200/270	8.7	0.150	3.2 (36.7%)	5.5 (63.3%)

* The value in the parenthesis is a fraction of this part of the acidity sites to total acidity sites.

3.4. Catalytic performance

We have found that L-phenylalaninol (L-p-ol) selectivity is independent on L-phenylalanine methyl ester (L-p) conversion over this CZA catalyst, and the formed L-p-ol does not undergo further reactions under the used conditions.[14] Hence, the L-p-ol selectivity (or yield) in

100 % conversion of L-p is used to describe the catalytic performances of the CZA-Mg$_x$ catalysts. The effect of the Mg^{2+} amount in the catalyst on its L-p-ol selectivity is presented in Fig. 8, in which a volcanic shape of the L-p-ol selectivity versus the Mg^{2+}/Al^{3+} molar ratio in the catalyst can be observed and the highest L-p-ol selectivity reached 91.2% over the CZA-0.1 catalyst.
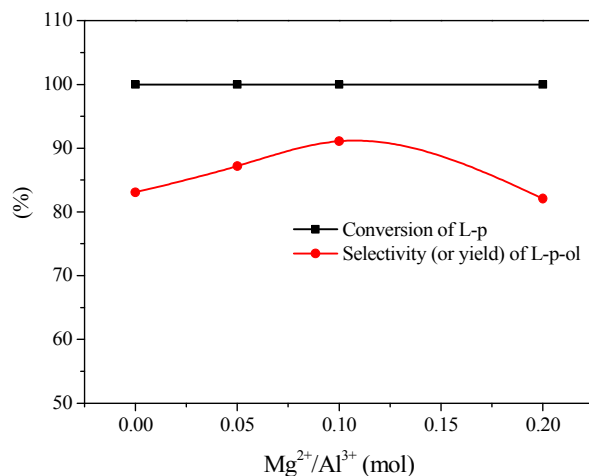

Fig. 8. The effect of Mg^{2+} content on the performance of the CuZn$_{0.3}$Mg$_x$AlO$_y$ catalysts at 110 °C and 4 MPa of H$_2$ for 5 h (L-p/Cat. =1.5, wt.). Experimental errors of the conversion and yield are within ±2%.
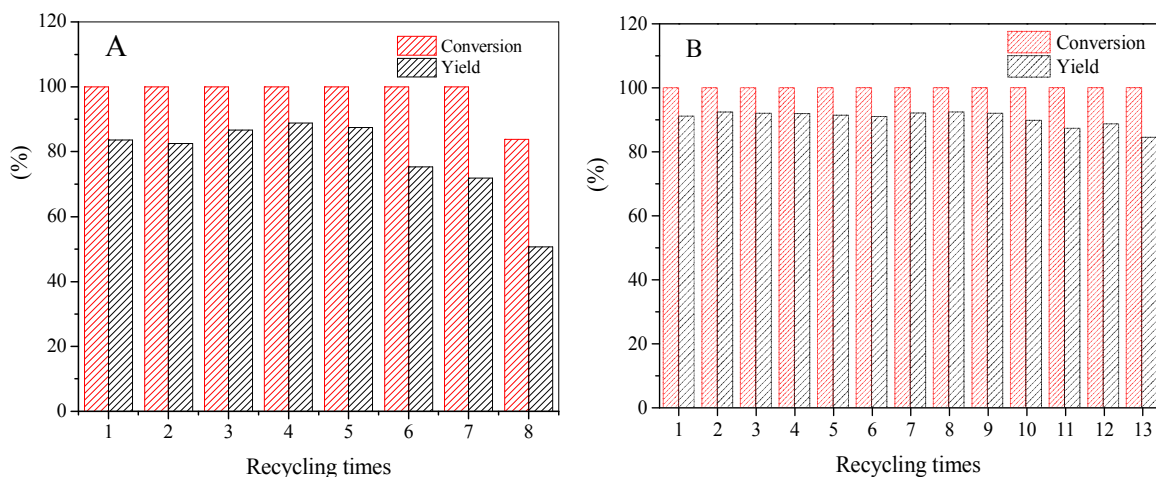

Fig. 9. The effect of recycling times on the catalytic activity of (A) CZA-0 and (B) CZA-0.1 catalysts for the hydrogenation of L-phenylalanine methyl ester at 110 °C and 4 MPa of H$_2$ for 5h (L-p/Cat. =1.5, wt.). Experimental errors of the conversion and yield are within ±2%.

Then, the CZA-0.1 catalyst was used as the model catalyst and its stability or property for recycling usage was tested, which was performed by repeating the batch operation under the optimum reaction conditions,[13] and the results are shown in Fig. 9. The results show that the catalytic activity of the CZA-0 catalyst dramatically decreased after run 7 times, the conversion of

L-Phenylalanine methyl ester was 83.7 % and the yield of L-phenylalaninol decreased to 50.7 %; the presence of Mg resulted in the great improvement of the stability of CZA-0.1 catalyst and after recycling utilization 13 times, the L-phenylalaninol selectivity of the CZA-0.1 catalyst was only decreased by 7.2%.

3.5. Discussion about the active sites on the catalyst

As a high-effective copper-based catalyst, a large metallic copper surface area (S_{Cu}) is generally thought as a prerequisite and the major goal in the catalyst preparation.[31,49-51] Recently, many researches have demonstrated that S_{Cu} is not the conclusive factor for the high catalytic activity. For instance, Spencer *et al.*[52] reported that the WGS reaction over the Cu/ZnO/Al$_2$O$_3$ catalyst was sensitive to some parameters of the catalyst other than its Cu surface area. Tan *et al.*[44] reported that the copper surface area or particle size of Cu and ZnO are not the decisive factors for the catalytic activity of the Cu/ZnO-based catalyst for the glycerol hydrogenolysis. Behrens *et al.*[53] investigated the role of the oxide component in the copper composite catalysts for the methanol synthesis, and found that the methanol synthesis rate is not only a function of the exposed Cu surface area alone in the hydrogenation of CO_2. Herein, to better disclose the relation between the catalytic activity and S_{Cu}, a plot of the L-p-ol selectivity versus S_{Cu} was presented in Fig. 10A. It can be seen that no direct linear correlation between the L-p-ol selectivity and S_{Cu} can be observed for this title reaction, which shows that the activity of the $CuZn_{0.3}Mg_xAlO_y$ catalyst is not only related to S_{Cu} but also to other causes. However, it also has to be mentioned that S_{Cu} is still an important parameter for the catalytic activity, because the CZA-0.2 sample has the smallest S_{Cu} and exhibits the lowest selectivity of L-p-ol.

Nowadays, it is widely accepted that Cu^0 is the active sites for hydrogenation reaction, but the nature of the active sites is still under debate. A lot of discussions about the influence of other intrinsic factors on the catalytic activity were reported, such as, the widely studied Cu-ZnO synergy [53,54], the SMSI effect between Cu^0 and the other oxides [18,56-59], the defects and steps of the Cu nanoparticles [56,60,61], the acidity and basicity of the catalysts [24,48,50], *etc*.
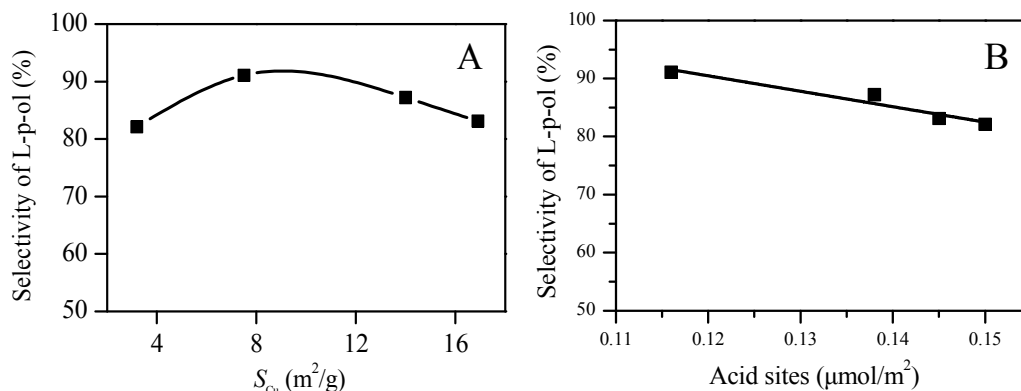
Fig. 10. The relations between the L-p-ol selectivity and (A) the Cu surface area, and (B) the density of total acidity sites.

We have found that there are some of the insoluble polyamide (by-product) on the surface and inside channels of the $CuZn_{0.3}AlO_x$ (CZA-0) catalyst after being used, which is an important reason for the decline of catalytic activity, as shown in Figs.S1 and S5, and Tables S1 and S2. And this insoluble polyamide can be formed catalytically on the acid sites, resulting in the active catalytic sites inaccessible to the reactants. The NH_3-TPD results show that the presence of MgO would reduce the acid sites of the catalyst to inhibit the formation of alkaline polyamide. Herein, the plot of the L-p-ol selectivity versus the density of total acidity sites was also taken and given in Fig. 10B. Obviously, the L-p-ol selectivity is decreased linearly with the increase in the density of total acidity sites. Hence, it can be concluded that these weaker acid sites are another importantly contributing factor for the increase of the catalytic activity and stability.

We also found that the deactivated $CuZn_{0.3}AlO_x$(CZA-0) catalyst have the larger size of the metallic copper crystallites (Figs. S2 and S3), resulting in the decline of the catalytic activity. In this $CuZn_{0.3}Mg_xAlO_y$ catalyst, the doping of Mg^{2+} ions can promote the formation of hydrotalcite-like phases in the precursor materials, which are beneficial to the atomically uniform distribution of the metallic oxides in hydrotalcite-like phases. The higher dispersion and smaller particle size of CuO species can be obtained after the hydrotalcite-like precursor materials were calcined. In these prepared platelet-like particles, the nanosized CuO species are to a large extent highly dispersed and embedded in the compact oxide matrix ($Zn_{0.3}Mg_xAlO_y$), which would decline the accessible Cu surface area. Moreover, this dense microstructure is beneficial to the SMSI effect between Cu^0 and

the other oxides after catalyst reduction, resulting in the decline of the reducibility of CuO species. On the one hand, this SMSI effect can act as an efficiently geometrical spacer and help to increase and stabilize the Cu^0 dispersion, which can prevent the agglomeration of Cu^0 particles during the reaction, to increase the catalytic activity and stability. On the other hand, an intimate interface contact of both catalyst components would enhance the SMSI effect between Cu^0 and ZnO, resulting in the migration of zinc atoms into the copper nanoparticle surfaces to further enhance the catalytic activity [53,56,60].

The results mentioned-above show that the high-effective $CuZn_{0.3}Mg_xAlO_y$ catalyst for the L-p-ol synthesis is mainly related to three essential factors: high S_{Cu}, appropriate SMSI effect and weaker acidity, and their relationship can be described as Fig. 11. The catalyst should possess a high S_{Cu} to expose a large number of active sites; by the help of the appropriate SMSI effect, increase and stabilize the Cu^0 dispersion and the active sites; and the catalyst's acidity should be weaker, which is beneficial to inhibit the formation of the insoluble polyamide and its desorption from the surface. Only if all three factors take effect together on this catalyst, the high-effective active sites would be formed for the hydrogenation of L-phenylalanine methyl ester to L-phenylalaninol.
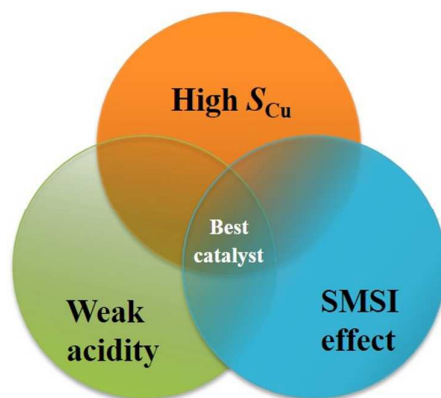

Fig. 11. Relationship of the essential factors for a high-effective L-p-ol synthesis catalyst.

4. Conclusions

In summary, a series of $CuZn_{0.3}Mg_xAlO_y$ (CZA-Mg$_x$, x = 0~0.2) catalysts derived from Cu-rich hydrotalcite-like compounds were prepared by co-precipitation method with Na_2CO_3 precipitant. The results show that the Mg^{2+} ions content has a significant influence on the physicochemical and

catalytic properties of the $CuZn_{0.3}Mg_xAlO_y$ catalysts for hydrogenation of L-phenylalanine methyl ester to L-phenylalaninol.

The introduction of Mg^{2+} ions in CZA can promote the formation of hydrotalcite-like precursors, and the Mg^{2+} ions content would affect the phase purity of hydrotalcite-like precursors. When the molar ratio of Mg^{2+}/Al^{3+} was 0.1, the phase-pure hydrotalcite-like precursor of $CuZn_{0.3}Mg_{0.1}AlO_y$ (CZA-0.1) catalyst can be obtained. With an increase in the Mg^{2+}/Al^{3+} molar ratio, the BET surface area and exposed copper surface area were decreased for CZA-Mg_x, and their amount of acid sites showed a similar change trend with Mg^{2+}/Al^{3+} molar ratio. The density of total acid sites of CZA-0.1 sample is the smallest and only 0.116 $\mu mol/m^2$.

The dense layered hydrotalcite-like precursors is beneficial to the atom-level distribution of corresponding metal oxides in the resulted $CuZn_{0.3}Mg_xAlO_y$ catalysts, and the stronger interaction between Cu^0 and Al_2O_3 (SMSI effect) after catalyst reduction can increase and stabilize the Cu^0 dispersion, resulting in the decrease in the CuO species reducibility.

The activity of the $CuZn_{0.3}Mg_xAlO_y$ catalyst is not only greatly dependent on the metallic copper surface area, but also the SMSI effect and the acidity of the catalysts. The CZA-0.1 catalyst with Mg^{2+}/Al^{3+} = 0.1 (mol) was made from the phase-pure hydrotalcite-like precursors and showed the highest activity among the CZA-Mg_x catalysts. When L-phenylalanine methyl ester was hydrogenated over this catalyst at 110 °C and 4 MPa of H_2, 100% conversion of L-phenylalanine methyl ester and 91.1 % yield of L-phenylalaninol without racemization were achieved. After recycling utilization 13 times, the L-phenylalaninol selectivity of the CZA-0.1 catalyst was only decreased by 7.2%, which shows its very high stability and recycling utilization property.

Acknowledgments

References

[1] C.L. Paradise, P.R. Sarkar, M. Razzak and J.K. De Brabander, *Org. Biomol. Chem.*, 2011, **9**, 4017-4020.

[2] J. Meng, G. Wei, X. Huang, Y. Dong, Y. Cheng and C. Zhu, *Polymer*, 2011, **52**, 363-367.

[3] J. Jiao, X. Liu, X. Mao, J. Li, Y. Cheng and C. Zhu, *New J. Chem.*, 2013, **37**, 317-322.

[4] A.R. Hajipour and F. Omidian, *High Perform. Polym.*, 2010, **22**, 550-566.

[5] A. Pinaka, G.C. Vougioukalakis, D. Dimotikali, E. Yannakopoulou, B. Chankvetadze and K. Papadopoulos, *Chirality*, 2013, **25**, 119-125.

[6] A.S. Saiyed and A.V. Bedekar, *Tetrahedron: Asymmetry*, 2013, *24*, 1035-1041.

[7] B. Ak, D. Elma, N. Meriç, C. Kayan, U. Işık, M. Aydemir, F. Durap and A. Baysal, *Tetrahedron: Asymmetry*, 2013, **24**, 1257-1264.

[8] S. Arita, T. Yabuuchi and T. Kusumi, *Chirality*, 2003, **15**, 609-614.

[9] H. HE, D. Gong and P. Wei, *Chem. Reagents*, 2005, **27**, 115-116.

[10] M.J. McKennon, A. Meyers, K. Drauz and M. Schwarm, *J. Org. Chem.*, 1993, **58**, 3568-3571.

[11] M. Souček, J. Urban and D. Šaman, *Collect. Czech. Chem. Commun.*, 1990, **55**, 761-765.

[12] R. Goncalves, A. Pinheiro, E. da Silva, J. da Costa, C. Kaiser and M. de Souza, *Synthetic Commun.*, 2011, **41**, 1276-1281.

[13] C. Gao, X. Xiao, D. Mao and G. Lu, *Catal. Sci. Technol.*, 2013, **3**, 1056-1062.

[14] Z. Shi, X. Xiao, D. Mao and G. Lu, *Catal. Sci. Technol.*, 2014, **4**, 1132-1143.

[15] G. Yang, N. Tsubaki, J. Shamoto, Y. Yoneyama and Y. Zhang, *J. Am. Chem. Soc.*, 2010, **132**, 8129-8136.

[16] S. Yu, Y. Chen, S. Gao, X. Wang and W. Huang, *Asian J. Chem.*, 2013, **25**, 6856-6860.

[17] S. Kaluza, M. Behrens, N. Schiefenhövel, B. Kniep, R. Fischer, R. Schlögl and M. Muhler, *ChemCatChem*, 2011, **3**, 189-199.

[18] M. Behrens, S. Zander, P. Kurr, N. Jacobsen, J.r. Senker, G. Koch, T. Ressler, R.W. Fischer and R. Schlögl, *J. Am. Chem. Soc.*, 2013, **135**, 6061-6068.

[19] M. Behrens, *J. Catal.*, 2009, **267**, 24-29.

[20] T. Fujitani and J. Nakamura, *Catal. Lett.*, 1998, **56**, 119-124.

[21] D.M. Whittle, A.A. Mirzaei, J.S. Hargreaves, R.W. Joyner, C.J. Kiely, S.H. Taylor and G.J. Hutchings, *Phys. Chem. Chem. Phys.*, 2002, **4**, 5915-5920.

[22] M. Turco, G. Bagnasco, U. Costantino, F. Marmottini, T. Montanari and G. Ramis, *J. Catal.*, 2004, **228**, 43-55.

[23] U. Costantino, M. Curini, F. Montanari, M. Nocchetti and O. Rosati, *Microp. Mesop. Mat.*, 2008, **107**, 16-22.

[24] P. Gao, F. Li, H. Zhan, N. Zhao, F. Xiao, W. Wei, L. Zhong, H. Wang and Y. Sun, *J. Catal.*, 2013, **298**, 51-60.

[25] P. Gao, F. Li, F. Xiao, N. Zhao, N. Sun, W. Wei, L. Zhong and Y. Sun, *Catal. Sci. Technol.*, 2012, **2**, 1447-1454.

[26] M. Behrens, I. Kasatkin, S. Kühl and G. Weinberg , *Chem. Mater.*, 2010, **22**, 386-397.

[27] J. Carpentier, S. Siffert, J. Lamonier, H. Laversin and A. Aboukaïs, *J. Porous Mat.*, 2007, **14**, 103-110.

[28] F. Cavani, F. Trifirò and A. Vaccari, *Catal. Today*, 1991, **11**, 173-301.

[29] M. Behrens, F. Girgsdies, A. Trunschke and R. Schlögl, *Eur. J. Inorg. Chem.*, 2009, **2009**, 1347-1357.

[30] C. Chen, P. Gunawan, X.W.D. Lou and R. Xu, *Adv. Funct. Mater.*, 2012, **22**, 780-787.

[31] X. Guo, D. Mao, G. Lu, S. Wang and G. Wu, *J. Catal.*, 2010, **271**, 178-185.

[32] L. He, H. Cheng, G. Liang, Y. Yu and F. Zhao, *Appl. Catal. A-Gen.*, 2012, **452**, 88-93.

[33] J. Cheng, J. Yu, X. Wang, L. Li, J. Li and Z. Hao, *Energy Fuels*, 2008, **22**, 2131-2137.

[34] R. Trujillano, M.J. Holgado, F. Pigazo and V. Rives, *Physica. B, Condensed Matter.*, 2006, **373**, 267-273.

[35] I. Melian-Cabrera, M.L. Granados and J. Fierro, *Phys. Chem. Chem. Phys.*, 2002, **4**, 3122-3127.

[36] C.-H. Zhou, J.N. Beltramini, C.-X. Lin, Z.-P. Xu, G.M. Lu and A. Tanksale, *Catal. Sci. Technol.*, 2011, **1**, 111-122.

[37] J.A. Gursky, S.D. Blough, C. Luna, C. Gomez, A.N. Luevano and E.A. Gardner, *J. Am. Chem. Soc.,* 2006, **128**, 8376-8377.

[38] R.K. Marella, C.K.P. Neeli, S.R.R. Kamaraju and D.R. Burri, *Catal. Sci. Technol.*, 2012, **2**, 1833-1838.

[39] M. Balaraju, K. Jagadeeswaraiah, P.S. Prasad and N. Lingaiah, *Catal. Sci. Technol.*, 2012, **2**, 1967-1976.

[40] M. Turco, G. Bagnasco, C. Cammarano, P. Senese, U. Costantino and M. Sisani, *Appl. Catal. B- Environ.*, 2007, **77**, 46-57.

[41] S. Murcia-Mascaros, R. Navarro, L. Gomez-Sainero, U. Costantino, M. Nocchetti and J. Fierro, *J. Catal.*, 2001, **198**, 338-347.

[42] S. Velu, K. Suzuki, M. Okazaki, M. Kapoor, T. Osaki and F. Ohashi, *J. Catal.*, 2000, **194**, 373-384.

[43] T. Shishido, M. Yamamoto, D. Li, Y. Tian, H. Morioka, M. Honda, T. Sano and K. Takehira, *Appl. Catal. A-Gen.,* 303 (2006) 62-71.

[44] H. Tan, M.N. Hedhill, Y. Wang, J. Zhang, K. Li, S. Sioud, Z.A. Al-Talla, M.H. Amad, T. Zhan and O.E. Tall, *Catal. Sci. Technol.*, 2013, **3**, 3360-3370.

[45] B. Li, G. Jin, J. Gao, R. Zhao, L. Dong and Y. Gong, *CrystEngComm*, 2014, **16**, 1253-1256 .

[46] S. Kühl, A. Tarasov, S. Zander, I. Kasatkin and M. Behrens, *Chem. Eur. J.,* 2014, **20**, 3782-3792.

[47] X. Long, Q. Zhang, Z.-T. Liu, P. Qi, J. Lu and Z.-W. Liu, *Appl. Catal. B-Environ.*, 2013, **134**, 381-388.

[48] D. Mao, W. Yang, J. Xia, B. Zhang, Q. Song and Q. Chen, *J. Catal.*, 2005, **230**, 140-149.

[49] A. Bienholz, H. Hofmann and P. Claus, *Appl. Catal. A-Gen.*, 2011, **391**, 153-157.

[50] X. Guo, D. Mao, G. Lu, S. Wang and G. Wu, *J. Mol. Catal. A-Chem.*, 2011, **345**, 60-68.

[51] S. Natesakhawat, J.W. Lekse, J.P. Baltrus, P.R. Ohodnicki Jr, B.H. Howard, X. Deng and C. Matranga, *ACS Catal.*, 2012, **2**, 1667-1676.

[52] G. Chinchen and M. Spencer, *Catal. Today*, 1991, **10**, 293-301.

[53] S. Zander, E.L. Kunkes, M.E. Schuster, J. Schumann, G. Weinberg, D. Teschner, N. Jacobsen, R. Schlögl and M. Behrens, *Angew. Chem. Int. Edit.*, 2013, **52**, 6536-6540.

[54] J.-D. Grunwaldt, A. Molenbroek, N.-Y. Topsøe, H. Topsøe and B. Clausen, *J. Catal.*, 2000, **194**, 452-460.

[55] M. Spencer, *Top. Catal.*, 1999, **8**, 259-266.

[56] M. Behrens, F. Studt, I. Kasatkin, S. Kühl, M. Hävecker, F. Abild-Pedersen, S. Zander, F. Girgsdies, P. Kurr and B.-L. Kniep, *Science*, 2012, **336**, 893-897.

[57] R.N. d'Alnoncourt, X. Xia, J. Strunk, E. Löffler, O. Hinrichsen and M. Muhler, *Phys. Chem. Chem. Phys.*, 2006, **8**, 1525-1538.

[58] Y. Xing, Z. Liu and S.L. Suib, *Chem. Mater.,* 2007, **19**, 4820-4826.

[59] J.-H. Lin, Z.-Y. Zeng, Y.-T. Lai and C.-S. Chen, *RSC Adv.*, 2013, **3**, 1808-1817.

[60] J.P. Greeley, *Science*, 2012, **336**, 810-811.

[61] T. Kandemir, F. Girgsdies, T.C. Hansen, K.D. Liss, I. Kasatkin, E.L. Kunkes, G. Wowsnick, N. Jacobsen, R. Schlögl and M. Behrens, *Angew. Chem. Int. Edit.*, 2013, **52**, 5166-5170

A high effective and stable $CuZn_{0.3}Mg_xAlO_y$ catalyst for the manufacture of chiral L-phenylalaninol: The role of Mg and its hydrotalcite-like precursor

Zhangping Shi, Shuangshuang Zhang, Xiuzheng Xiao, Dongsen Mao and Guanzhong Lu*
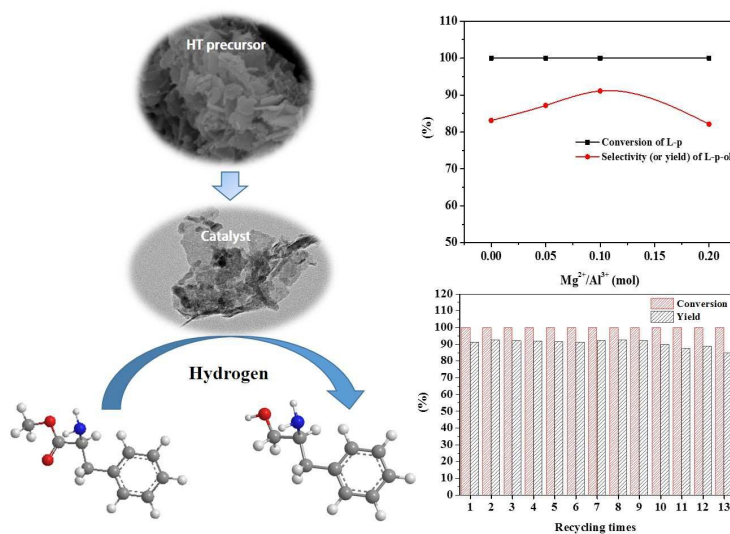
A High-effective and stable $CuZn_{0.3}Mg_{0.1}AlO_y$ catalyst derived from Cu-rich hydrotalcite-like precursor was prepared for the catalytic hydrogenation of L-phenylalanine methyl ester to L-phenylalaninol with ~100% ee selectivity.